Wind-Induced Effect on Octagonal Building Interfered by Square Buildings in 'T' Pattern

Rony Kar and Sujit Kumar Dalui

1 Introduction

The responses of the tall buildings due to wind excitation can be found out by either wind tunnel experiment or computational fluid dynamics (CFD) analysis. While the wind tunnel experiment gives reliable results, it is cumbersome, costly and time-consuming, whereas CFD simulation is relatively cheaper and less time tedious. Though there is debate among researchers about the reliability of this method, it can be easily overcome by validating a small part of the analysis with wind tunnel results and adopting modern analysis methods and practices. In the past decade, many researchers have investigated the effect of wind excitation on tall structures by either wind tunnel study or CFD simulation, some of which are briefly highlighted here. Some researchers have performed aerodynamic and aeroelastic analyses on the Commonwealth Advisory Aeronautical Council (CAARC) standard tall building model using numerical CFD simulation to explore a competent and reliable approach for evaluation of wind effects [1–3]. A few sets of wind tunnel experiments have been carried out to determine aerodynamic forces and wind pressures acting on square plan tall building models with various configurations like corner cut, setbacks, helical, etc. [4]. Different sets of triangular and square plan buildings with corner modifications are also investigated under wind excitation [5]. Irregular plan-shaped (e.g. E shape, Y shape, etc.) tall buildings are also subjected to wind load to find out their responses [6, 7]. It can be noted that research is scarce on wind interference effects on tall buildings except for square or rectangular plan-shaped buildings. Some of the works of the literature are briefly described here. Interference effects on peak pressure coefficients between rectangular and square plan-shaped buildings have been investigated [8,

R. Kar (✉) · S. K. Dalui
Department of Civil Engineering, Indian Institute of Engineering Science and Technology, Shibpur, Howrah, India

9]. Mittal et al. [10] and Behera et al. [11] studied interference effects on wind-induced responses for two square tall buildings with varying orientation and plan ratio. The wind interference effects between two oval plan-shaped buildings [12] and interference effect on an array of tall buildings [13] are evaluated. Lo and Kim [14] studied interference effect on a square plan and tapered buildings, whereas Sy et al. [15] examined wind over top flow between two square plan-shaped buildings. Liang et al. [16] studied the wind interference effects of a ventilated supertall building on a neighbouring supertall building.

Very few studies are conducted for investigating the interference effect on the octagonal plan-shaped tall building [17, 18]. In the current study, the interference effect on an octagonal plan-shaped tall building due to the presence of three tall buildings of square plan shape for 0°–360° wind incidence angles is investigated. The four buildings are arranged in 'T' pattern for this particular study. This specific building arrangement has been chosen to explore the effect on the principal building, due to interfering buildings positioned at the side and downstream of the principal building. The variations of force and pressure coefficients due to change in wind angle and the presence of interfering buildings are portrayed.

2 Numerical Analysis

The principal octagonal plan-shaped tall building and the square plan-shaped interfering buildings are 30 m in width and 150 m in height. The buildings are arranged in 'T' configuration with a distance of 60 m among them. A model scale of 1:300 is used for creating the domain and building models. The building set-up with the face nomenclature for the octagonal building is depicted in Fig. 1. The wind incidence angle θ is varied from 0° to 360°, as shown in the figure.

The analyses are conducted by numerical simulation by Ansys CFX using shear stress transport (SST) turbulence model prescribed by Menter [19]. The governing equations and the boundary conditions for the SST turbulence model are as follows. Here, k = turbulence kinetic energy and ω = the rate of dissipation of the eddies.

$$\frac{\partial(\rho k)}{\partial t} + \frac{\partial(\rho u_j k)}{\partial x_j} = P - \beta^* \rho \omega k + \frac{\partial}{\partial x_j}\left[(\mu + \sigma_k \mu_t)\frac{\partial k}{\partial x_j}\right] \qquad (1)$$

$$\frac{\partial(\rho \omega)}{\partial t} + \frac{\partial(\rho u_j \omega)}{\partial x_j} = \frac{\gamma}{v_t} P - \beta \rho \omega^2 + \frac{\partial}{\partial x_j}\left[(\mu + \sigma_\omega \mu_t)\frac{\partial \omega}{\partial x_j}\right]$$
$$+ 2(1 - F_1)\frac{\rho \sigma_{\omega^2}}{\omega}\frac{\partial k}{\partial x_j}\frac{\partial \omega}{\partial x_j} \qquad (2)$$

where

Fig. 1 T pattern building
configuration in the
interference condition
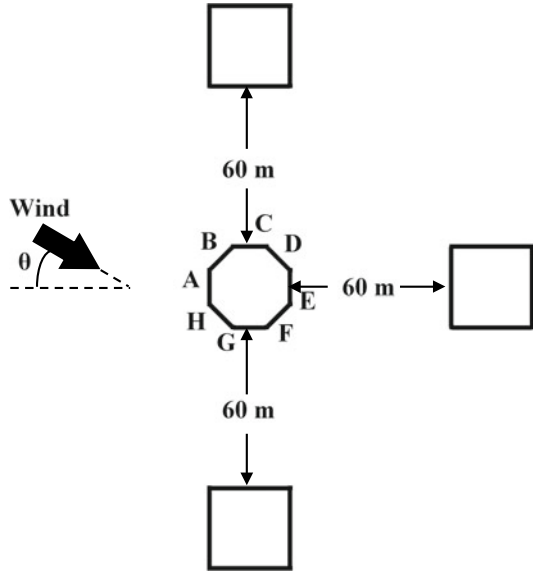
$$P = \tau_{ij}\frac{\partial u_i}{\partial t} \tag{3}$$

$$\tau_{ij} = \mu_t\left(2S_{ij} - \frac{2}{3}\frac{\partial u_k}{\partial x_k}\delta_{ij}\right) - \frac{2}{3}\rho k\delta_{ij} \tag{4}$$

$$S_{ij} = \frac{1}{2}\left(\frac{\partial u_i}{\partial x_j} + \frac{\partial u_j}{\partial x_i}\right) \tag{5}$$

$$\mu_t = \frac{\rho a_1 k}{\max(a_1\omega, \Omega F_2)} \tag{6}$$

$$\Phi = F_1\Phi_1 + (1 - F_1)\Phi_2 \tag{7}$$

$$F_1 = \tanh\left(\arg_1^4\right) \tag{8}$$

$$\arg_1 = \min\left[\max\left(\frac{\sqrt{k}}{\beta^*\omega d}, \frac{500\nu}{d^2\omega}\right), \frac{4\rho\sigma_{\omega^2}k}{CD_{k\omega}d^2}\right] \tag{9}$$

$$CD_{k\omega} = \max\left(2\rho\sigma_{\omega^2}\frac{1}{\omega}\frac{\partial k}{\partial x_j}\frac{\partial\omega}{\partial x_j}, 10^{-20}\right) \tag{10}$$

$$F_2 = \tanh\left(\arg_2^2\right) \tag{11}$$

$$\arg_2 = \max\left(\frac{\sqrt{k}}{\beta^*\omega d}, \frac{500\nu}{d^2\omega}\right) \tag{12}$$

Constants:

$$\sigma_{k_1} = 0.85, \sigma_{\omega_1} = 0.65, \beta_1 = 0.075$$
$$\sigma_{k_2} = 1.00, \sigma_{\omega_2} = 0.856, \beta_2 = 0.0828$$
$$\beta^* = 0.09, a_1 = 0.31$$

Boundary and far-field conditions:
Far field

$$\frac{U_\infty}{L} < \omega_{\text{farfield}} < 10\frac{U_\infty}{L} \tag{13}$$

$$\frac{10^{-5}U_\infty^2}{R_e L} < k_{\text{farfield}} < 0.1\frac{U_\infty^2}{R_e L} \tag{14}$$

Boundary conditions:

$$\omega_{\text{wall}} = 10\frac{6\nu}{\beta_1(\Delta d_1)^2} \tag{15}$$

$$k_{\text{wall}} = 0 \tag{16}$$

However, following the Wilcox formulation, Ansys CFX disregards the factor of 10 for eddy rate dissipation at the wall.

The computational domain is constructed by following the recommendation of Franke et al. [20]. The atmospheric boundary layer (ABL) is simulated using the power law equation by considering open terrain with scattered obstructions. The generation of the boundary layer and the computational domain's construction is performed, as mentioned by Kar and Dalui [17].

For validation purpose, the velocity profile and turbulence intensity (I) profile found by SST turbulence model in the isolated condition are compared with that from wind tunnel test in Dalui [21]. This comparison is depicted in Fig. 2, and good agreement is seen for both the parameters.

2.1 Grid Convergence Test

A grid convergence test has been executed to check the employed meshing's effectiveness to deliver precise wind-induced responses. The principal building in the 'T'
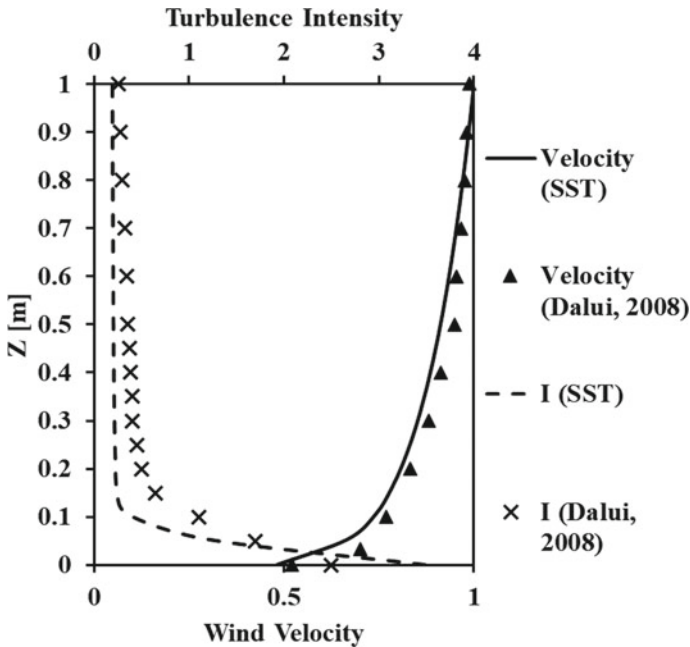
Fig. 2 Comparison of velocity and turbulence intensity profile

pattern building configuration under 0° wind incidence angle is analysed for various mesh densities, and the force coefficients are calculated for the different cases. The optimum mesh density is found where the values of the force coefficients converge. The mesh generation in other cases is performed using this optimum mesh density. The grid convergence test is compiled in Fig. 3. Here, case 5 has been taken as optimum meshing as the error is negligible and valuable computational resources and time can be saved using it.

3   Results and Discussion

The study on the interference cases of the octagonal building for varying wind incidence angles is analysed, and the wind-induced responses are compared. The wind-induced responses of the principal building are compared to differentiate between stand-alone and interfering conditions. The flow visualization of the isolated and interfering cases under some typical wind incidence angles is shown in Fig. 4. The difference in flow pattern around the set-up and the vortices at the wake of the principal building are evident for different cases.
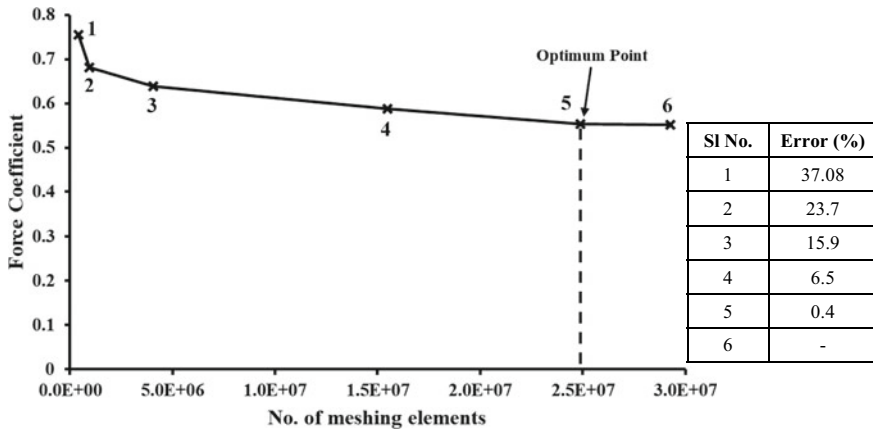
Sl No.	Error (%)
1	37.08
2	23.7
3	15.9
4	6.5
5	0.4
6	-

Fig. 3 Grid convergence test for T pattern building configuration

3.1 Force Coefficients

The variation of drag coefficient with respect to wind incidence angle in both inter-fering and isolated conditions is shown in Fig. 5a. The maxima for drag coefficient for both isolated and interfering cases are at 0° and 180° wind incidence angles. A massive variation between isolated and interference conditions is noted between 150° and 210° wind angles. The presence of the interfering buildings at the side and downstream of the principal building is the main reason for this. The maximum difference in drag coefficients between both the cases is 46% at 180° wind angle.

The variation of lift coefficient with respect to the wind incidence angle between interfering and isolated conditions is shown in Fig. 5b.

The maxima for lift coefficient for the isolated case are at 90° and 270° wind incidence angles. The peak values for interference case, however, occur at 45°, 165°, 195° and 315°. A huge variation between isolated and interference conditions is noted between the 60° and 300° wind angle regions. The interfering buildings' presence at the side and downstream of the principal building induces this huge difference. The maximum difference in lift coefficients between both the cases is 149% at 165° and 195° wind angles. It can be observed that the difference in lift coefficient for isolated and interfering buildings is more pronounced than the drag coefficient. So, the side and downstream interfering buildings contribute more to the across-wind effect than along-wind effect.
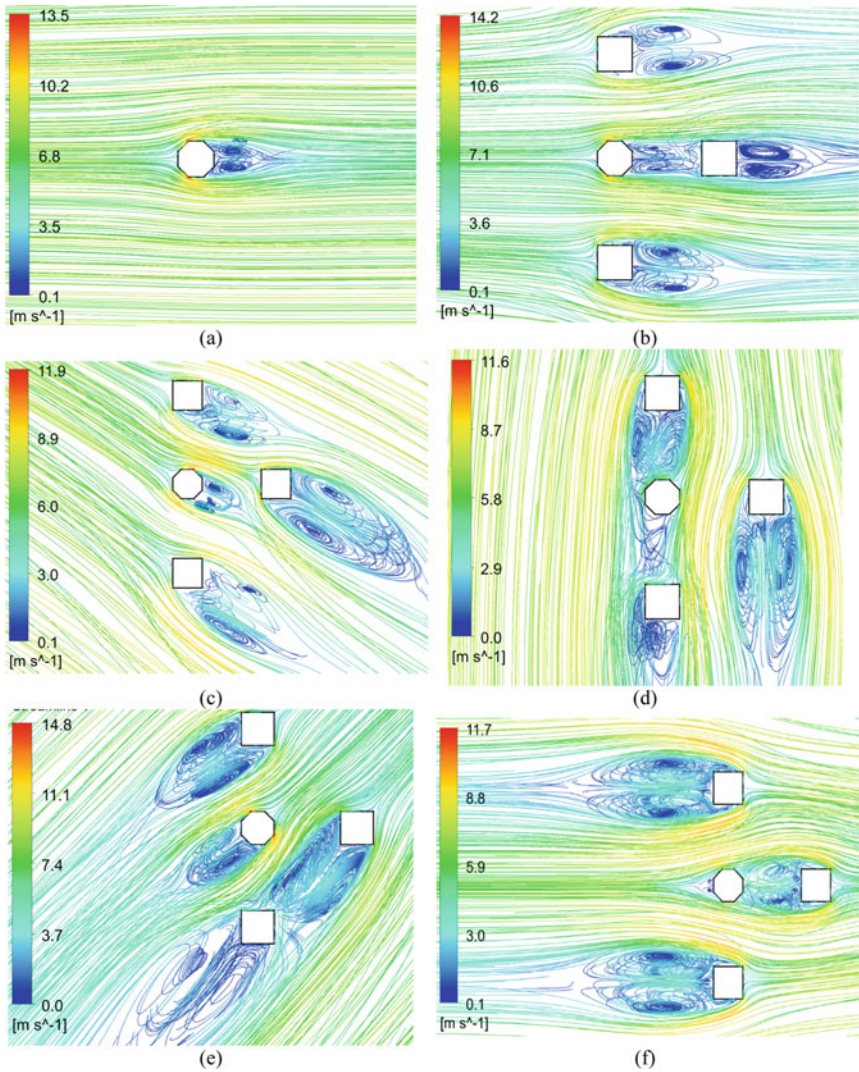
Fig. 4 Flow pattern for **(a)** isolated case and interference condition for **(b)** 0°, **(c)** 30°, **(d)** 90°, **(e)** 135° and **(f)** 180° wind incidence angles

3.2 Pressure Coefficients

Pressure coefficients for each face of the octagonal building are defined as follows.

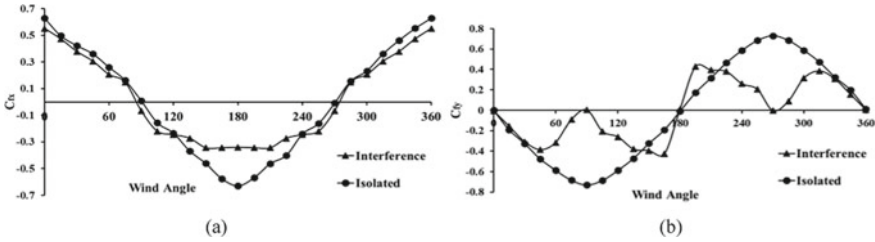$$C_\text{p} = \frac{\text{Average pressure over the area of a building face}}{0.6 V_z^2} \tag{16}$$

Fig. 5 Comparison of **(a)** drag coefficient and **(b)** lift coefficient in isolated and interference condition

where C_p is the pressure coefficient for each face and V_z is the approach velocity of wind.

The variation of pressure coefficients (C_p) with respect to wind angle for the isolated and interfering case is shown in Fig. 6. A noteworthy difference can be observed on all the octagonal building faces between isolated and interference cases.

A significant variation between C_p of the isolated case and interference case on Face A is observed for 75°–285° wind angles. The maximum change is 77% at wind angles 90° and 270°. It is due to the presence of the side interfering buildings. Relatively smaller variation has noted rest of the wind angles. The region of somewhat greater interference for Face B is also ranged from 75° to 285° wind angles. In this case, 129% variation is noted at wind angle 75°. For Face C, the maximum interference ranges between 60° and 180° wind angles. The peak variation is 228% at a wind angle of 120°.

For Face D, the region of most considerable interference lies between 165° and 225° wind incidence angles. A maximum variation of 156% is noted at a wind angle of 165°. For Face E, the maximum interference occurs between 75° and 285° wind incidence angles. A considerable deviation of 228% is observed at 150° and 210° wind angles. The maximum interference region for Face F is from 135° to 195° wind angles. A peak variation of 163% is spotted at 195° wind incidence angle. The region of most significant interference for Face G lies between 75° and 300° wind angles. The variation is highest at 240° wind angle with a deviation of 232%. The greatest interference for Face H is noted from 75° to 285° wind angles. The maximum variation of 129% is observed at 285° wind incidence angle. The difference of C_p for a face, between isolated and interfering cases, is maximum when there is an interfering building present between the wind flow and the principal building. The variation also depends upon the effect of the building set-up on the flow characteristics around the principal building. It can be observed that, due to the presence of the interfering buildings at the sides and downstream of the principal building, the maximum interference is caused between 75° and 300° wind angles for all the faces. The regions of wind incidence angle 0°–60° and 300°–360° exhibit the least amount of interference due to the absence of interfering building to the direct upstream of the principal building.
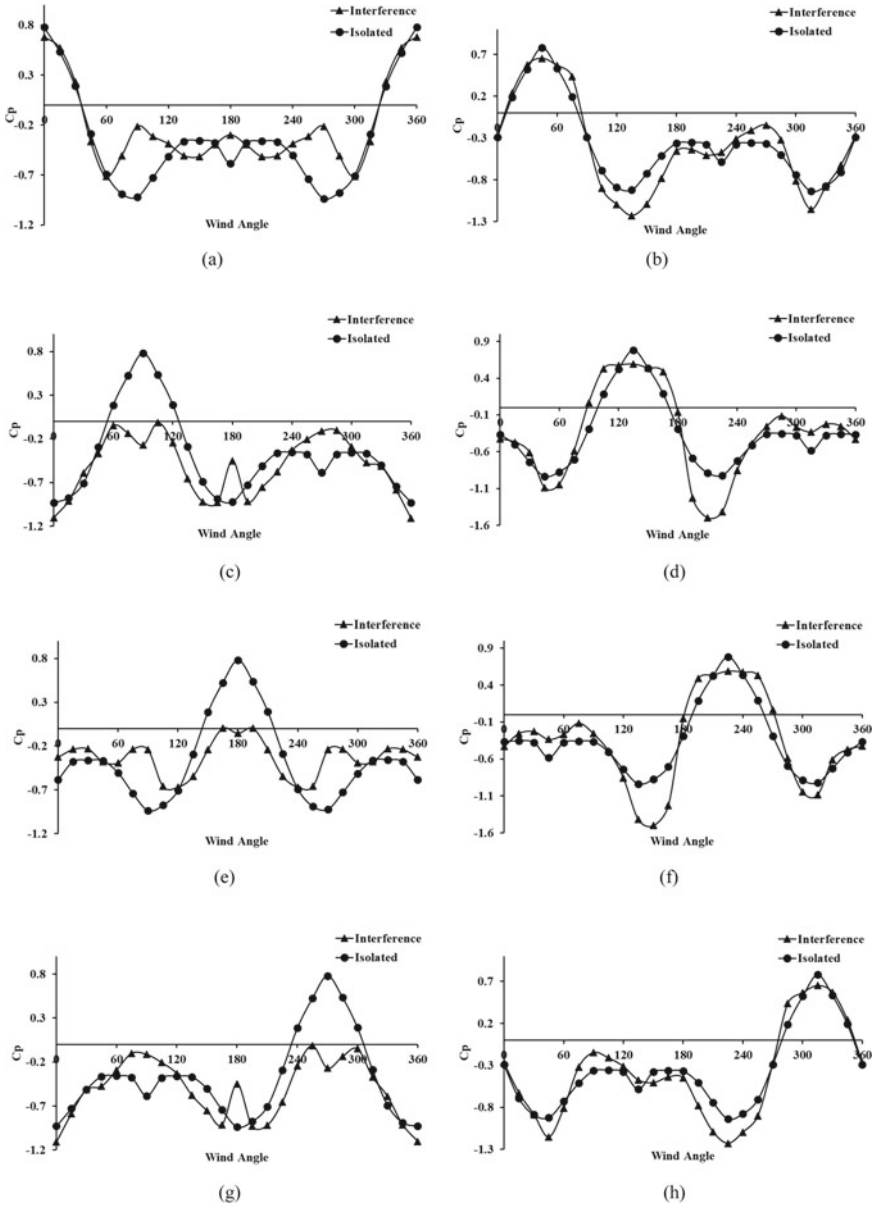
Fig. 6 Variation of pressure coefficient with wind angle for **(a)** Face A, **(b)** Face B, **(c)** Face C, **(d)** Face D, **(e)** Face E, **(f)** Face F, **(g)** Face G and **(h)** Face H for isolated and interference condition

4   Conclusion

The flow pattern around the set-up and the vortices at the wake of the principal building vary greatly for different wind angles in interference case. The principal building's drag coefficient does not exhibit any noteworthy difference between isolated and interference conditions except for 150°–210° wind angles. The drag coefficient is maximum for both isolated and interference conditions at 180° wind angle. The peak difference in drag coefficients between isolated and interference conditions is 46% at 180° wind angle. The lift coefficient, however, differs significantly between isolated and the interference conditions. The lift coefficient exhibits its maxima at 90° and 270° wind incidence angles for an isolated case. A huge variation is seen between both the cases for wind angles 60°–300°. The maximum difference in lift coefficient between both conditions is 149% at 165° and 195°. So, the interfering buildings for this 'T' configuration contribute more to the across-wind effect than along-wind effect. A notable difference in mean pressure coefficients for the isolated and interfering state is observed for all the faces of the principal building. The deviation is especially significant for faces C, D, E, F and G. The peak deviation of pressure coefficients between isolated and interfering buildings varies from 77 to 232% on various faces of the principal building.

References

1. Huang S, Li QS, Xu S (2007) Numerical evaluation of wind effects on a tall steel building by CFD. J Constr Steel Res 63(5):612–627. https://doi.org/10.1016/j.jcsr.2006.06.033
2. Braun AL, Awruch AM (2009) Aerodynamic and aeroelastic analyses on the CAARC standard tall building model using numerical simulation. Comput Struct 87(9–10):564–581. https://doi.org/10.1016/j.compstruc.2009.02.002
3. Abu-Zidan Y, Mendis P, Gunawardena T (2020) Impact of atmospheric boundary layer inhomogeneity in CFD simulations of tall buildings. Heliyon 6(7):e04274. https://doi.org/10.1016/j.heliyon.2020.e04274
4. Tanaka H, Tamura Y, Ohtake K, Nakai M, Chul Kim Y (2012) Experimental investigation of aerodynamic forces and wind pressures acting on tall buildings with various unconventional configurations. J Wind Eng Ind Aerodyn 107–108:179–191 (2012). https://doi.org/10.1016/j.jweia.2012.04.014
5. Baghaei Daemei A, Rahman Eghbali S (2019) Study on aerodynamic shape optimisation of tall buildings using architectural modifications in order to reduce wake region. Wind Struct Int J 29(2):139–147. https://doi.org/10.12989/was.2019.29.2.139
6. Bhattacharyya B, Dalui SK (2018) Investigation of mean wind pressures on 'E' plan shaped tall building. Wind Struct Int J 26(2):99–114
7. Mukherjee S, Chakraborty S, Dalui SK, Ahuja AK (2014) Wind induced pressure on 'Y' plan shape tall building. Wind Struct Int J 19(5):523–540. https://doi.org/10.12989/was.2014.19.5.523
8. Hui Y, Tamura Y, Yoshida A (2012) Mutual interference effects between two high-rise building models with different shapes on local peak pressure coefficients. J Wind Eng Ind Aerodyn 104–106:98–108. https://doi.org/10.1016/j.jweia.2012.04.004

9. Hui Y, Yoshida A, Tamura Y (2013) Interference effects between two rectangular-section high-rise buildings on local peak pressure coefficients. J Fluids Struct 37:120–133. https://doi.org/10.1016/j.jfluidstructs.2012.11.007

10. Mittal H, Sharma A, Gairola A (2019) Investigation of pedestrian-level wind environment near two high-rise buildings in different arrangements. Adv Struct Eng 22(12):2620–2634. https://doi.org/10.1177/1369433219849832

11. Behera S, Ghosh D, Mittal AK, Tamura Y, Kim W (2020) The effect of plan ratios on wind interference of two tall buildings. Struct Des Tall Spec Build 29(1):2–11. https://doi.org/10.1002/tal.1680

12. Zhao DX, He BJ (2017) Effects of architectural shapes on surface wind pressure distribution: case studies of oval-shaped tall buildings. J Build Eng 12:219–228. https://doi.org/10.1016/j.jobe.2017.06.009

13. Mohammad AF, Zaki SA, Ikegaya N, Hagishima A, Ali MSM (2018) A new semi-empirical model for estimating the drag coefficient of the vertical random staggered arrays using LES. J Wind Eng Ind Aerodyn 180:191–200. https://doi.org/10.1016/j.jweia.2018.08.003

14. Lo Y, Kim YC (2019) Estimation of wind-induced response on high-rise buildings immersed in interfered flow. J Appl Sci Eng 22(3):429–448. https://doi.org/10.6180/jase.201909

15. Sy LD, Yamada H, Katsuchi H (2019) Interference effects of wind-over-top flow on high-rise buildings. J Wind Eng Ind Aerodyn 187:85–96. https://doi.org/10.1016/j.jweia.2019.02.001

16. Liang R, Xu A, Zhao R (2020) Wind interference effects of a ventilated supertall building on its neighboring supertall building—a case study. Struct Des Tall Spec Build 29(7):1–21. https://doi.org/10.1002/tal.1725

17. Kar R, Dalui SK (2016) Wind interference effect on an octagonal plan shaped tall building due to square plan shaped tall buildings. Int J Adv Struct Eng 8(1):73–86. https://doi.org/10.1007/s40091-016-0115-z

18. Kar R, Dalui SK, Bhattacharjya S (2019) An efficient optimisation approach for wind interference effect on octagonal tall building. Wind Struct Int J 28(2). https://doi.org/10.12989/was.2019.28.2.111

19. Menter FR (1994) Two-equation eddy-viscosity turbulence models for engineering applications. AIAA J 32(8):1598–1605. https://doi.org/10.2514/3.12149

20. Franke J et al (2004) Recommendations on the use of CFD in wind engineering. In: Cost action C, Jan 2004, pp 1–11

21. Dalui SK (2008) Wind effects on tall buildings with peculiar shapes. Doctoral dissertation. Indian Institute of Technology Roorkee, Roorkee, India. Retrieved from http://shodhbhagirathi.iitr.ac.in:8081/xmlui/handle/123456789/1633